Research Square

Preprints are preliminary reports that have not undergone peer review.
They should not be considered conclusive, used to inform clinical practice,
or referenced by the media as validated information.

pH-responsive tanshinone IIA-loaded hydrogel nanoparticles inducing ferroptosis, autophagy and apoptosis for anticancer treatment

Yuefeng Zhang
Liaocheng University
Jing Wang
liaocheng people's hospital
Lijun Mu
Liaocheng University
Yingxin Ma
Liaocheng University
Ru Li
Liaocheng University
Pan Li
Liaocheng University
Tianying Ren
dxmei_312@163.com
Liaocheng University
Lusha Ji
Liaocheng University

Article

Keywords: Tanshinone II A, calcium alginate hydrogel, autophagy, ferroptosis, apoptosis

Posted Date: May 6th, 2024

DOI: https://doi.org/10.21203/rs.3.rs-4321007/v1

License: This work is licensed under a Creative Commons Attribution 4.0 International License. Read Full License

Additional Declarations: No competing interests reported.

Abstract

Tanshinone IIA (Tan IIA) is a lipophilic active constituent derived from the rhizomes and roots of Salvia miltiorrhiza Bunge (Danshen), a Chinese medicinal herb. However, Tan IIA suffers from low absorption and limited bioavailability due to its poor solubility in water. To address this issue, we utilized calcium alginate hydrogel (CA) as a hydrophilic carrier for Tan IIA, enabling enhance the solubility. Besides, the nanoparticles, with pH-responsive property may have great potential on controlled drug delivery. The Tan IIA/CA nanoparticles also exhibited significant anticancer activity in vitro. Furthermore, we investigated the molecular mechanisms underlying the anticancer effect of Tan IIA/CA, revealing the involvement of apoptosis, ferroptosis, and autophagy pathways. This study not only confirms the anticancer properties of Tan IIA/CA, but also provides novel insights and strategies for enhancing the solubility of poorly water-soluble compounds.

1. Introduction

Cancer currently stands as the predominant cause of mortality in the human population, with its global incidence continuing to rise[1]. Chemotherapy remains the primary therapeutic approach for addressing malignant tumors[2]. Nonetheless, the effectiveness of chemotherapy is constrained by the development of resistance to drugs and the occurrence of severe and undesirable toxic effects [3–5]. As a consequence, the identification and development of novel antitumor medications assume critical importance and require immediate attention.

Tanshinone IIA (Tan IIA) is a lipophilic active compound that is derived from the rhizomes and roots of the Chinese medicinal herb Salvia miltiorrhiza Bunge (Danshen)[6]. Its pharmacological properties have made it a popular choice for the treatment of cardiovascular diseases[7, 8]. Moreover, Tan IIA exhibits a diverse array of biological effects, including anti-inflammatory and anticancer activities[9, 10]. In fact, it has been utilized as an antitumor agent against various types of cancer cells, including lung cancer, breast cancer, and glioma[11–13].

Natural Tan II A has been shown to have poor bioavailability due to its low water solubility, first-pass metabolism, and inadequate dissolution rates, which hinder its clinical application[14, 15]. The insolubility and insufficient dissolution rates of Tan II A pose significant challenges. In order to enhance the solubility of Tan II A, a water-soluble derivative called sodium tanshinone IIA sulphonate (sodium tanshinone IIA sulphonate injection) was developed and is currently being used clinically for the treatment of cardiovascular diseases. However, this structural modification has led to a decrease in the antitumor activities of Tan IIA[16, 17]. Therefore, it is necessary and meaningful to explore a technology that does not involve altering the structure of Tan II A.

Multiple drug carriers have recently been developed to enhance the water solubility of anticancer drugs, including hydrogels[18]. Smart hydrogels are capable of responding to environmental stimuli such as heat, light, and pH, enabling in situ gelation and controlled drug release [19, 20]. This feature significantly improves the convenience and efficiency of drug delivery [21, 22]. Alginate, a widely studied polysaccharide, has been extensively investigated for topical drug delivery due to its low toxicity and adjustable properties[22, 23]. The hydrophilic polymer has already received approval from the US Food and Drug Administration for biomedical applications [24, 25]. Alginate hydrogels can be easily fabricated by crosslinking sodium alginate in a calcium chloride aqueous solution [26]. Additionally, alginate hydrogels offer numerous advantages, including non-immunogenic and biodegradable properties, gel formation under mild conditions, adjustable degradation rate, and biocompatibility [27, 28]. These qualities make alginate hydrogels suitable candidates for encapsulating drugs and anticancer agents.

This study describes the preparation of Tan II A/CA nanoparticles using a modified water-in-oil (w/o) emulsion solvent diffusion method. The loading of Tan II A onto these nanoparticles were achieved through a simple, low-cost procedure that demonstrated good repeatability and scalability. The Tan II A/CA nanoparticles exhibited pH-responsive characteristics and displayed robust antitumor cell activity based on in vitro cell apoptosis experiments. In addition, the antitumor mechanisms of these nanoparticles were investigated. Overall, Tan II A/CA nanoparticles have potential as anticancer drugs.

2. Materials and methods

2.1 Materials

Sodium alginate (SA), calcium chloride ($CaCl^2$), doxorubicin (DOX), and tanshinone IIA were purchased from Macklin. Dulbecco's Modified Eagle Medium (DMEM), trypsin, fetal bovine serum (FBS), phosphate-buffered saline (PBS), and penicillin-streptomycin (PS) solution were purchased from Procell (Beijing, China). Polyvinylidene fluoride (PVDF) membranes were purchased from Millipore. RIPA lysis buffer, phenylmethanesulfonyl fluoride (PMSF) (a serine protease inhibitor), protein-loading buffer, biomarkers, and primary antibodies (GPX4, GAPDH, Caspase 3) and secondary antibodies were purchased from Abcam Biotech (Shanghai, China). Cell Counting Kit-8 (CCK-8) was purchased from Dingguo Biology (Beijing, China).

2.2 Preparation of calcium-alginate nanoparticles

The nanoparticles were prepared using a modified water-in-oil emulsification process, as described in the literature [29]. To prepare the nanospheres, a 1 mL solution of 1% sodium alginate was emulsified with sunflower oil containing 2 mL of span 80 for 30 minutes using an oscillator set at a speed of 2000 rpm. The resulting emulsions were promptly transferred to a mixture of sunflower oil and glacial acetic acid in a 1:1 ratio, and stirred at 200 rpm for 15 minutes at room temperature. In a separate step, 30 mL of a 1 mol/L $CaCl_2$ solution was added to the mixture and vigorously agitated for 2 hours. Subsequently, the mixtures were centrifuged at 7000 rpm for 10 minutes. The supernatant was discarded, and the pellet containing the nanospheres was suspended in isopropyl alcohol to remove any remaining sunflower oil. The nanospheres were then washed twice with 10 mL portions of a 1 mol/L $CaCl_2$ solution, with each wash being accompanied by gentle vortex mixing for 10 minutes. Finally, the nanospheres were suspended in a 1 mol/L $CaCl_2$ solution and stored at 4°C.

2.3 Pharmaceutical characterization

The hydrodynamic size of nanoparticles in distilled water was measured using dynamic light scattering (DLS) with the Malvern Zetasizer Nano. To prepare the samples, zirconia-stabilized yttria dry powder was mixed with distilled water and cell culture medium (DMEM with 10% FBS), achieving a concentration of 60 μg/mL. The resulting suspension was sonicated at room temperature for 15 minutes at 20 W using a sonicator. Subsequently, the hydrodynamic size was determined.

2.4 Encapsulation efficiency and loading efficiency

For the treatment of Dox and Tan IIA samples, 1mL of double distilled water (ddH2O) was combined with the tested sample. The resulting solution was then subjected to analysis using a Nanodrop 2000 spectrophotometer.

Drug loading content (%) = Weight of DOX or Tan IIA calculated /Weight of nanoparticles ×100

Encapsulation efficiency (%) = Weight of DOX or Tan /Weight of total DOX or Tan×100

The drug concentration in the solution was measured using a UV–vis spectrophotometer at a wavelength of 250 nm.

2.5 Cell culture

The CX 1 and HGC 27 cell lines were obtained from the Cell Bank of the Chinese Academy of Sciences and subjected to STR DNA profiling. The cells were grown in DMEM medium supplemented with 10% FBS and 1% PS, and maintained in a 37°C incubator with 5% CO^2.

2.6 CCK 8 assay

Cells were seeded into 96-well plates at a density of 1×10^5 cells/mL and cultured in 100 μL of DMEM medium for 24 hours. Subsequently, nanoparticles were introduced into the plates, followed by the addition of CCK-8 solution. The optical density (OD) at 450 nm was measured after a 2-hour incubation period.

2.7 Flow cytometry analysis

Cells were seeded into 6-well plates at a density of 1×10^5 cells/mL, and nanoparticles were added overnight. Afterward, cells were washed with PBS and collected by trypsin treatment. Subsequently, these cells were stained with the 7-AAD Annexin V apoptosis detection kit following the manufacturer's instructions, and analyzed using a BD flow cytometer. Each experiment was performed in triplicate.

2.8 Western blots assay

For the western blot assay, cells were seeded into 6 cm cell dishes at a density of 1×10^5 cells/mL for 24 hours. The cells were then washed with PBS three times and lysed using RIPA buffer and protease inhibitors. The protein concentration was determined using a BCA protein assay kit. An equal amount of total protein was loaded onto SDS-PAGE gels and subsequently transferred to a PVDF membrane. The PVDF membrane was blocked using quick blotting buffer for 10 minutes and washed three times with TBST buffer. Next, the PVDF membrane was incubated with the primary antibody, followed by a secondary antibody conjugated with Horseradish Peroxidase. The blots were visualized using the Bio-rad ChemiDoc Imager. All western blots were performed in triplicate as independent experiments, with GAPDH chosen as the internal reference.

2.9 Cell migration assay

Migration ability was assessed using a scratch migration assay in which 5×10^4 cells/mL were seeded in 3.5 cm cell dishes and incubated for 24 h. A vertical scratch was created using a pipette tip, and the width of the scratch was measured at 0 h and 24 h.

2.10 Measurement of intracellular Ca^{2+} level

The cells were cultured in 12-well dishes for 24 hours. Subsequently, the cells were treated with 5 mM of flur 3 in order to monitor the alterations in intracellular Ca^{2+} levels. The changes were observed using an inverted confocal laser scanning microscopy. Furthermore, the fluorescent intensity of the stained cells was assessed through flow cytometry (BD Arial III), utilizing an excitation wavelength of 488 nm.

2.11 Confocal imaging of cells

Cells were seeded in 6-well plates at a density of 1×10^5 cells/mL and incubated for 24 hours. The nanoparticles carrying doxorubicin (DOX) were then added to the cells for a 2-hour period. Following this, the cells were fixed in 4% paraformaldehyde. Confocal images of the cells were obtained using a Leica laser scanning confocal microscope.

2.12 Fourier-transform infrared (FTIR)

The absorption spectra were evaluated using a Varian 3000 Fourier Transform Infrared (FTIR) spectrophotometer. The FTIR technique was employed to characterize the chemical properties of the calcium alginate hydrogel.

2.13 Transmission electron microscopy (TEM)

Cell suspension was prepared by digesting cells with trypsin, followed by fixation in 4% paraformaldehyde for a minimum of 12 hours. Subsequently, an examination of the cells was conducted using a JEM-1400 transmission electron microscope.

2.14 Statistical analysis

The experiments were conducted in three independent replicates. The data were presented as mean ± standard error. A one-way analysis of variance (ANOVA) and Tukey test were used to compare the control and experimental groups. P values < 0.05 were considered statistically significant.

2.15 RNA extraction and Transcriptome sequencing

Transcriptome sequencing were performed by Sangon Biotec Corporation (Shanghai, China). Briefly, total RNA was extracted from the frozen samples of two replicates using Trizol reagent (Sangon, China). RNA integrity and pollution were detected on 1% agarose gel electrophoresis. RNA concentration was measured using Qubit RNA Assay Kit (Life Technologies). mRNA was enriched and purified from the total RNA using mRNA Capture Beads, and then broken into short fragments. The first- and second-strand cDNA fragments were synthesized after reverse transcription reaction. The double-stranded cDNAs were enriched and purified by Hieff NGS™ DNA Selection Beads. The double-stranded cDNAs were used for end reparation, poly(A) addition, and ligation with sequencing DNA adaptors. Following purification and size selection, cDNA libraries were generated from appropriate size of DNA fragments using Super CanaceTM High-Fidelity Mix Kit. The quality of cDNA libraries was detected Qubit DNA Assay Kit. Finally, the cDNA libraries were sequenced on an Illumina NovaSeq6000 platform.

2.16 Sequence assembly, functional annotation and classification

Base calling was transferred to sequenced reads (i.e., raw reads). The quality of sequencing data was evaluated by checking the distributions of the sequencing error rate and A/T/G/C content. Meanwhile, reads with an adapter, reads with 'N' base, low quality reads with a Qphred ≤ 20, length less than 35nt and their paired reads were removed. The remaining reads were clean reads. Transcriptome assembly was performed using Trinity software (Grabherr et al., 2011). Gene function annotation was analyzed by BLASTX alignment against the NR (NCBI non-redundant protein database), KEGG (Kyoto encyclopedia of genes and genomes), Pfam, and GO (Gene Ontology) databases (E-value ≤ 1e-5). The gene expression levels were estimated with TPM (Transcripts Per Million). The p-value < 0.05 and the log2(Treat/Control) > 1.5 were used as the threshold to discriminate the DEGs (differential gene expression).

3. Results and discussions

3.1 Preparation of nanoparticles

In order to characterize interactions between the drugs (Tan IIA) and carriers, the FTIR spectrum of pure Tan IIA, Tan IIA/CA and CA hydro polymers were investigated (Fig. 2A). The FTIR spectrum of Tan IIA/CA were the superposition of spectra of Tan IIA and CA nanoparticle. Analysis of the spectra for either Tan IIA/CA or individual components did not show any changes for the specific absorption band for the polymers or the Tan IIA, demonstrating that there were no chemical interactions between Tan IIA and CA nanoparticles.

Tan IIA/CA particles were synthesized by the modified W/O emulsion cation method and the nanoparticles size was characterized by DLS analysis (Fig. 2B). Hydrated nanoparticles displayed a larger particle size due to water absorption and swelling, with size ranging from 200 to 400 nm.

3.2 Drug encapsulation and release in vitro

To evaluate the efficacy of CA hydrogel carriers, we conducted an analysis of drug encapsulation and release rates. The drug encapsulation rate were 47.8 ± 5.6% and 40.2 ± 5.1% respectively for DOX and Tan IIA while the loading capacities were 40.2 ± 5.1% and 40.2 ± 5.1% (Table 1).

Table 1
The encapsulation efficiency and loading capacity of DOX/CA and Tan IIA/CA particles.

Particles	Encapsulation efficiency%	Loading capacity %
DOX/CA	57.8 ± 5.6	46.5 ± 3.2
Tan IIA/CA	50.2 ± 5.1	42.4 ± 4.5

Furthermore, we assessed the release patterns of Tan IIA/CA to investigate the drug release behavior in CA hydrogels. The cumulative release amount at pH 2.4 and pH 8.6 exceeded 60% (Fig. 3). Notably, a rapid release occurred within 30 minutes at pH 2.4 and pH 8.6, indicating that changes in pH can trigger the release of Tan IIA. Conversely, the release amount was less than 20% at pH 4.4 and pH 7.8 (Fig. 3). These findings collectively demonstrate the remarkable pH-responsive characteristics of CA hydrogels.

3.3 Nontoxic properties

To confirm the non-toxicity of the hydrogel, CCK-8 assays were conducted to assess cell proliferation. Cells were cultured in the presence and absence of CA hydrogels for a duration of 4 days. The results of the CCK-8 assays indicated that there was no substantial variance in cell viability between the experimental and control groups (Fig. 4A). In order to analyze whether calcium alginate microspheres may cause changes in intracellular calcium ion concentration, Ca^{2+} concentration were analyzed by Flow cytometry. There was no significantly increase observed in free intracellular calcium concentrations ($p > 0.05$) (Fig. 4B). Consequently, these findings demonstrate the biocompatibility of the CA nanocarriers with the tested cells.

3.4 Drug uptake ability in vitro

To investigate the cellular uptake capability of CA nanoparticles, we employed Dox as the targeted drug, owing to its intrinsic fluorescence. As depicted in Figure xx, the drug was observed to be rapidly internalized by the cells. Furthermore, the fluorescence intensity exhibited by the Dox/CA groups was found to be significantly greater when compared to the control groups (Fig. 5A). The controlled groups, in this experiment, consisted of blank CA nanoparticles. Subsequent Hoechst 33327 staining revealed that Dox not only successfully reached the nucleus but also indicated the ability of the drug to traverse the nuclear membrane.

The fluorescence signals in cellular samples were analyzed using flow cytometry, and the corresponding results are presented in Fig. 5B. The figure clearly illustrates that the fluorescence intensity observed in the Dox/CA groups is significantly stronger than that observed in the control groups. These findings are in line with the results obtained from the confocal microscope analysis.

To confirm the uptake of drugs by cells, we conducted scanning electron microscopy (SEM) analysis as depicted in Fig. 6A. In this particular experiment, we utilized Tan IIA/CA nanoparticles as our experimental groups. The nanoparticles were observed within the plasma of the cells treated with Tan IIA/CA nanoparticles. Consequently, these findings collectively indicate that the uptake of CA nanoparticles by cells is facilitated.

3.5 Anticancer ability in vitro

The cell killing ability of Tan IIA/CA nanoparticles was assessed in vitro using CCK8 assays and flow cytometry assays. The CCK8 assays demonstrated a significant decrease in cell proliferation ability in the groups treated with Tan IIA/CA (Fig. 6B). Flow cytometry analysis of cell apoptosis revealed a significant increase in cell apoptosis in the groups treated with Tan IIA/CA nanoparticles compared to the control groups (Fig. 6C). Scanning electron microscopy (SEM) was performed as shown in Fig. 6A, which revealed the presence of nanoparticles in the plasma of cells treated with Tan IIA/CA nanoparticles. These cells treated with Tan IIA/CA nanoparticles exhibited altered morphology, showing shrinkage and cell membrane rupture. Furthermore, cell scratch assay showed that Tan IIA/CA decreased cell migration significantly after 48h incubation (Fig. 6D and E). These results demonstrate that the Tan IIA/CA can effectively against tumor cells.

3.6 Transcriptomic analyses

To found the mechanisms of anticancer effects induced by Tan IIA/CA, transcriptomic analyses were performed. We constructed eight cDNA libraries from the control group (H1, H2, C1, and C2) and Tan IIA treatment group (HT1, HT2, CT1 and CT2), respectively (Table 2). After removing adaptor sequences, low-quality and ambiguous “N” sequences, transcriptome sequencing generated 214,801,546 clean reads and 3.1×10^{10} bp in group HT vs H of HGC27 cancer cells, with more than 51,000,000 reads and 7.4×10^{9} bp per sample. Meanwhile a total of 200,076,854 reads and 2.8×10^{10} bp was acquired from group CT vs C of CX1 cancer cells, with more than 44,000,000 reads and 6.4×10^{9} bp per sample. Average reads were at least 144 bp in length per sample. The Q20 values of reads were greater than 98.8%. Q30 scores were over 96.2% in all samples. The contents of GC ranged from 52.6 to 54.4%. These values indicated a high quality of clean reads.

Table 2
Summary of RNA-seq clean data in group HT *vs* H of HGC27 cancer cells and group CT vs C of CX1 cancer cells. Abbreviations: CT: CX 1 cells treated with IIA/CA.

Sample	HT1	HT2	HT3	H1	H2	H3	CT1	CT2	CT3
Total Reads Count(#)	55590646	51585078	55087862	51282474	56343348	53812911	44685862	49494306	47090084
Total Bases Count(bp)	8018322967	7455267812	773679538	7466638761	8170208380	7818423571	6479365295	7172275399	6825820347
Average Read Length(bp)	144.24	144.52	144.45	145.6	145.01	145.3	145	144.91	144.96
Q10 Bases Count(bp)	8001423705	7439545492	772048462	7449007281	8151318468	7800162875	6461773661	7151595460	6806684561
Q10 Bases Ratio(%)	99.79%	99.79%	99.7%	99.76%	99.77%	99.7%	99.73%	99.71%	99.71%
Q20 Bases Count(bp)	7952826783	7394373331	767360026	7397235782	8096391117	7746813450	6409958787	7091490487	6750724637
Q20 Bases Ratio(%)	99.18%	99.18%	99.1%	99.07%	99.10%	99.1%	98.93%	98.87%	98.97%
Q30 Bases Count(bp)	7798359715	7251470951	752491533	7231616645	7920864107	7576240376	6245530856	6900969339	6573250098
Q30 Bases Ratio(%)	97.26%	97.27%	97.2%	96.85%	96.95%	96.92%	96.39%	96.22%	96.95%
N Bases Count(bp)	433618	367761	400689	362907	438470	400689	312621	367599	340110
N Bases Ratio(%)	0.01%	0.00%	0.00%	0.00%	0.01%	0.00%	0.00%	0.01%	0.00%
GC Bases Count(bp)	4261930436	3997774689	412985256	4012761140	4300578456	415666980	3524789488	3844896391	3684842940
GC Bases Ratio(%)	53.15%	53.62%	53.41%	53.74%	52.64%	53.72%	54.40%	53.61%	53.82%

3.6 Differentially expressed genes (DEGs)

To compare the DEGs in group HT vs H of HGC27 cancer cells and group CT vs C of CX1 cancer cells, we identified DEGs with volcano plots (Fig. 7). In all, 1418 genes were identified as DEGs in group HT vs H, of which 254 DEGs were significantly up-regulated and 1164 DEGs were significantly down-regulated (Fig. 6A). According to the results of transcriptome analysis, we obtained 567 DEGs in group CT vs C, of which 287 were up-regulated and 280 were down-regulated (Fig. 6B).

3.7 Gene Ontology (GO) analyses and KEGG pathway analyses of DEGs

To explore the biological functions of the DEGs, GO (Gene Ontology) functional annotation and KEGG (Kyoto Encyclopedia of Genes and Genomes) enrichment analysis was conducted. First, we performed GO functional annotation of DEGs of in group HT vs H of HGC27 cancer cells. The DEGs were classified into three main categories and further divided into 62 functional subgroups in group HT vs H (Fig. 8A). In biological process (BP), these genes were predominantly distributed into cellular process (GO:0009987), biological regulation (GO:0065007), regulation of biological process (GO:0050789), and metabolic process (GO:0008152). In cellular component (CC), cell (GO:0005623) and cell part (GO:0044464) are significantly enriched GO terms, followed by organelle (GO:0043226). In molecular function (MF), the majority of DEGs were involved in binding (GO:0005488) and catalytic activity (GO:0003824). For KEGG pathway enrichment analysis, DEGs of group HT vs H were significantly enriched in 24 pathways, which are related to apoptosis, autophagy, cellular senescence, ferroptosis, and immune system (Fig. 8C). Of them, PI3K-Akt signaling pathway (ko04151), Regulation of actin cytoskeleton (ko04810), MAPK signaling pathway (ko04010), Calcium signaling pathway (ko04020), Ras signaling pathway (ko04014), Rap1 signaling pathway (ko04015), Focal adhesion (ko04510), Cell cycle (ko04110), and cGMP-PKG signaling pathway (ko04022) were the highly enriched pathways.

Subsequently, we conducted GO functional annotation and KEGG pathway enrichment analysis to characterize the roles of DEGs in group CT vs C of CX1 cancer cells. The DEGs were enriched with 58 functional subgroups in group CT vs C, including 25 GO terms in the BP category, 20 GO terms in the CC category, and 13 terms in the MF category (Fig. 8B). In BP category, DEGs were mainly annotated in cellular process (GO:0009987), biological regulation (GO:0065007), metabolic process (GO:0008152), regulation of biological process (GO:0050789), and response to stimulus (GO:0050896). In CC category, these unigenes were predominantly distributed into cell (GO:0005623) and cell part (GO:0044464), organelle (GO:0043226), and membrane (GO:0016020). In MF category, binding (GO:0005488) and catalytic activity (GO:0003824) had the largest numbers of DEGs. For the KEGG pathway enrichment analysis, we found that the DEGs of group CT vs C were mainly classified into 32 pathways, which are related to immune system, autophagy, ferroptosis, and apoptosis (Fig. 8D). The significant pathway was PI3K-Akt signaling pathway (ko04151), MAPK signaling pathway (ko04010), Focal adhesion (ko04510), Calcium signaling pathway (ko04020), Regulation of actin cytoskeleton (ko04810), Rap1 signaling pathway (ko04015), Circadian entrainment (ko04713), Ras signaling pathway (ko04014), JAK-STAT signaling pathway (ko04630), TNF signaling pathway (ko04668), Glutamatergic synapse (ko04724) and Chemokine signaling pathway (ko04062).

To further verify these results, we performed WB in seven differentially expressed proteins (GPX4, Caspase 3, ATG 5, AMPK, phosphorylated AMPK, mTOR and phosphorylated mTOR). GPX4 is a key protein to inhibit ferroptosis and declines of GPX4 induces ferroptosis. Caspase 3 plays a key role in induced apoptosis and ATG 5 is a key protein involved in autophagy. Moreover, AMPK/mTOR signlaing pathway is a key signaling pathway involved in autophagy. WB results showed that increased levels of ATG 5, Caspase 3 and decreased level of GPX4, AMPK, phosphorylated AMPK, mTOR and phosphorylated mTOR either in HGC 27 or CX 1 cells treated with Tan IIA/CA. These results also reveal that Tan IIA/CA perform anti-tumor functions through promoting apoptosis, autophagy and ferroptosis. These results are consistent with those results of second generation sequencing.

4. Discussion

Tan IIA is an important fat-souble compositons of Salvia mitiorrhiza, which has been widely used for treating various cardiovascular diseases and also has antitumor effect. Poorly water-soluble drugs are a common obstacle in pharmaceutical development, presenting a significant challenge. The limited solubility of these drugs often leads to suboptimal bioavailability and reduced therapeutic effectiveness. Consequently, increasing efforts have been dedicated to improving the solubility of poorly water-soluble drugs. This is done in order to enhance their overall performance and optimize drug delivery, ultimately resulting in improved therapeutic outcomes. The CA nanoparticles were synthesized using an improved method [29]. As illustrated in Fig. 1, a Tan IIA/CA drug delivery system were prepared. Nanoparticles are manufactured by W/O emulsification technique. In order to improve loading capacity of Tan IIA/CA, we first synthesized drug free nanoparticles (CA) and then encapsulation of Tan IIA was carried out by mixing Tan IIA with CA nanoparticles. As previous studies have shown that CA hydrogels have characteristics of pH responsive and biocompatibility [30]. In alkaline conditions calcicum alginate nanoparticles showed drug release ability due to its simultaneously swelling and degradation [31, 32]. In pH 2 condition calcicum alginate nanoparticles exhibited drug release ability due to matrix shrinkage [31, 33]. Tan IIA/CA in this research also displays same characteristics, response to dual pH. With the ability to respond to changes in pH, Tan IIA/CA can therefore facilitate accurate and controlled release of drugs.

Since nanoparticles have pH responsive, we selected human gastric cancer cell line (HGC 27) and colorectal cancer cell line (CX 1) as our research objects. Colon pH is alkaline (pH 8.3–8.4) and gastric pH is acidic [34]. In vitro experiments demonstrate that Tan IIA exerts its anti-tumor activity against HGC 27 and CX 1 cancer cells. This is consistent with previous studies [35]. However, the mechanisms of Tan IIA antitumor activity remain unclear.

Concerned that CA nanoparticles contained Ca^{2+}, we analyzed intracellular calcium concentrations with flow cytometry. There was no significantly change in levels of Ca^{2+} ions. These results proved that the anticancer effects of Tan IIA/CA are not correlated with CA carriers.

In vitro experiments Tan IIA/CA significantly inhibited cell proliferation and reduced migration of HGC 27 and CX 1 cells. The mechanistic study revealed that the anticancer effect of Tan IIA/CA can exert anti-tumor effects by regulating ferroptosis and apoptosis. We also verified these results at the protein level by WB. Increased expression of Caspase 3 and decreased expression of GPX4 proteins were observed. AMPK/mTOR signal pathway are key signaling pathways involved in regulating autophagy [36]. AMPK is verified to be a promoter of autophagy and it inhibits mTOR activity to promote autophagy in cancer progression[37]. Ferroptosis is believed to be regulated by AMPK signaling pathway, and activation of AMPK/mTOR inhibits ferroptosis[38]. In our research

Tan IIA/CA also induced autophagy through AMPK/mTOR signal pathway in the same way. Although we screened the molecular mechanisms of Tan IIA/CA induced antitumor and some signaling pathway were confirmed in this study, these underlying antitumor mechanisms of Tan IIA/CA are poorly understood. In this study we analyzed significantly changing gene functions and the corresponding pathways with GO and KEGG enrichment analyses. Our data showed that the most significantly involved pathways were apoptosis, autophagy, cellular senescence, ferroptosis, and immune system. Our data verified the involvement of apoptosis, autophagy and ferroptosis in the antitumor mechanisms of Tan IIA/CA. Molecular details of immune system will need further elaborations.

Taken together, our findings suggested that Tan IIA can suppress cancer cell growth, migration, and invasion as well as promote cell apoptosis. Tan IIA plays a role as an antitumor agent. our findings support the use of Tan IIA as an antitumor drug. Our findings also provide significant evidence supporting the continued exploration and advancement of Tan IIA/CA as a therapeutic agent for the treatment of cancers.

5. Conclusions

This study revealed that calcium alginate hydrogel is a strategy to improve insolubility of Tanshinone IIA. Furthermore, we observed that calcium alginate hydrogel has good characteristic of pH-responsive, biocompatibility and nontoxicity. Our findings not only establish an effective approach but also elucidate the molecular mechanism underlying Tanshinone IIA induced antitumor. Tanshinone IIA can exert antitumor effects by promoting cell apoptosis, autophagy and ferroptosis. These results provide a scientific foundation for designing controlled release of anticancer drugs and application of Tanshinone IIA as cancer drugs. Further research may encourage the use of this technique in formulating alginatenanocapsules for Tanshinone IIA encapsulation and controlled release targeted in anti-tumor area.

Declarations

Declaration of competing interest

The authors declare that there are no conflicts of interest.

Data availability statement

Data is provided within the manuscript or supplementary information files.

Acknowledgments

This work was supported by Shandong Provincial Natural Science Foundation, China (No. ZR202102180037).

Author Contribution

Yuefeng Zhang and Jing Wang wrote the original manuscript and prepared figures 1 -8. Lijun Mu and Yingxin Ma cultured cells and prepared Figure 3-4. Ru Li and Pan Li analyzed data and prepared Figure 5. Tianying Ren and Lusha Ji design experiments and edited manuscript. Lusha Ji offered foundation for this study. All authors reviewed the manuscript.

References

1. Mattiuzzi C, Lippi G. Current Cancer Epidemiology. J Epidemiol Glob Health. 2019;9(4):217-222. Https://doi.org/10.2991/jegh.k.191008.001
2. Tilsed CM, Fisher SA, Nowak AK, Lake RA, Lesterhuis WJ. Cancer chemotherapy: insights into cellular and tumor microenvironmental mechanisms of action. Front Oncol. 2022;12:960317.Https://doi.org/10.3389/fonc.2022.960317
3. Li J, Wang R, Gao J. Novel anticancer drugs approved in 2020. Drug Discov Ther. 2021;15(1):44-47.Https://doi.org/10.5582/ddt.2021.01013
4. Liu YP, Zheng CC, Huang YN, He ML, Xu WW, Li B. Molecular mechanisms of chemo- and radiotherapy resistance and the potential implications for cancer treatment. MedComm (2020). 2021;2(3):315-340.Https://doi.org/10.1002/mco2.55
5. Brianna, Lee SH. Chemotherapy: how to reduce its adverse effects while maintaining the potency? Med Oncol. 2023;40(3):88.Https://doi.org/10.1007/s12032-023-01954-6
6. Yang C, Mu Y, Li S, Zhang Y, Liu X, Li J. Tanshinone IIA: a Chinese herbal ingredient for the treatment of atherosclerosis. Front Pharmacol. 2023;14:1321880.Https://doi.org/10.3389/fphar.2023.1321880
7. Jiang Q, Chen X, Tian X, et al. Tanshinone I inhibits doxorubicin-induced cardiotoxicity by regulating Nrf2 signaling pathway. Phytomedicine. 2022;106:154439.Https://doi.org/10.1016/j.phymed.2022.154439
8. Lai Z, He J, Zhou C, Zhao H, Cui S. Tanshinones: An Update in the Medicinal Chemistry in Recent 5 Years. Curr Med Chem. 2021;28(14):2807-2827.Https://doi.org/10.2174/0929867327666200521124850
9. Li H, Hu P, Zou Y, et al. Tanshinone IIA and hepatocellular carcinoma: A potential therapeutic drug. Front Oncol. 2023;13:1071415.Https://doi.org/10.3389/fonc.2023.1071415
10. Guo R, Li L, Su J, et al. Pharmacological Activity and Mechanism of Tanshinone IIA in Related Diseases. Drug Des Devel Ther. 2020;14:4735-4748.Https://doi.org/10.2147/DDDT.S266911

11. Li W, Huang T, Xu S, et al. Molecular Mechanism of Tanshinone against Prostate Cancer. Molecules. 2022;27(17).Https://doi.org/10.3390/molecules27175594
12. Zhou J, Jiang YY, Chen H, Wu YC, Zhang L. Tanshinone I attenuates the malignant biological properties of ovarian cancer by inducing apoptosis and autophagy via the inactivation of PI3K/AKT/mTOR pathway. Cell Prolif. 2020;53(2):e12739.Https://doi.org/10.1111/cpr.12739
13. Zhou X, Pan Y, Wang Y, et al. Tanshinones induce tumor cell apoptosis via directly targeting FHIT. Sci Rep. 2021;11(1):12217.Https://doi.org/10.1038/s41598-021-91708-z
14. Ashour AA, Ramadan AA, Abdelmonsif DA, El-Kamel AH. Enhanced oral bioavailability of Tanshinone IIA using lipid nanocapsules: Formulation, in-vitro appraisal and pharmacokinetics. Int J Pharm. 2020;586:119598.Https://doi.org/10.1016/j.ijpharm.2020.119598
15. Meng Z, Meng L, Wang K, et al. Enhanced hepatic targeting, biodistribution and antifibrotic efficacy of tanshinone IIA loaded globin nanoparticles. Eur J Pharm Sci. 2015;73:35-43.Https://doi.org/10.1016/j.ejps.2015.03.002
16. Zhai X, Li C, Lenon GB, Xue CCL, Li W. Preparation and characterisation of solid dispersions of tanshinone IIA, cryptotanshinone and total tanshinones. Asian J Pharm Sci. 2017;12(1):85-97.Https://doi.org/10.1016/j.ajps.2016.08.004
17. Chu T, Zhang Q, Li H, et al. Development of intravenous lipid emulsion of tanshinone IIA and evaluation of its anti-hepatoma activity in vitro. Int J Pharm. 2012;424(1-2):76-88.Https://doi.org/10.1016/j.ijpharm.2011.12.049
18. Bhaladhare S, Bhattacharjee S. Chemical, physical, and biological stimuli-responsive nanogels for biomedical applications (mechanisms, concepts, and advancements): A review. Int J Biol Macromol. 2023;226:535-553.Https://doi.org/10.1016/j.ijbiomac.2022.12.076
19. Fugolin APP, Huynh B, Rajasekaran SP. Innovations in the Design and Application of Stimuli-Responsive Restorative Dental Polymers. Polymers (Basel). 2023;15(16).Https://doi.org/10.3390/polym15163346
20. Khan F, Atif M, Haseen M, et al. Synthesis, classification and properties of hydrogels: their applications in drug delivery and agriculture. J Mater Chem B. 2022;10(2):170-203.Https://doi.org/10.1039/d1tb01345a
21. Gao S, Tang G, Hua D, et al. Stimuli-responsive bio-based polymeric systems and their applications. J Mater Chem B. 2019;7(5):709-729.Https://doi.org/10.1039/c8tb02491j
22. Lee KY, Mooney DJ. Alginate: properties and biomedical applications. Prog Polym Sci. 2012;37(1):106-126.Https://doi.org/10.1016/j.progpolymsci.2011.06.003
23. Abka-Khajouei R, Tounsi L, Shahabi N, Patel AK, Abdelkafi S, Michaud P. Structures, Properties and Applications of Alginates. Mar Drugs. 2022;20(6).Https://doi.org/10.3390/md20060364
24. Li J, Mooney DJ. Designing hydrogels for controlled drug delivery. Nat Rev Mater. 2016;1(12).Https://doi.org/10.1038/natrevmats.2016.71
25. Chenthamara D, Subramaniam S, Ramakrishnan SG, et al. Therapeutic efficacy of nanoparticles and routes of administration. Biomater Res. 2019;23:20.Https://doi.org/10.1186/s40824-019-0166-x
26. Zhou Z, Wang J, Jiang C, et al. Advances in Hydrogels for Meniscus Tissue Engineering: A Focus on Biomaterials, Crosslinking, Therapeutic Additives. Gels. 2024;10(2).Https://doi.org/10.3390/gels10020114
27. Jacob S, Nair AB, Shah J, Sreeharsha N, Gupta S, Shinu P. Emerging Role of Hydrogels in Drug Delivery Systems, Tissue Engineering and Wound Management. Pharmaceutics. 2021;13(3).Https://doi.org/10.3390/pharmaceutics13030357
28. Sarmento B, Ribeiro A, Veiga F, Sampaio P, Neufeld R, Ferreira D. Alginate/chitosan nanoparticles are effective for oral insulin delivery. Pharm Res. 2007;24(12):2198-2206.Https://doi.org/10.1007/s11095-007-9367-4
29. Fernando IPS, Kirindage K, Jeon HN, Han EJ, Jayasinghe AMK, Ahn G. Preparation of microspheres by alginate purified from Sargassum horneri and study of pH-responsive behavior and drug release. Int J Biol Macromol. 2022;202:681-690.Https://doi.org/10.1016/j.ijbiomac.2022.01.171
30. Liu H, Cai Z, Wang F, et al. Colon-Targeted Adhesive Hydrogel Microsphere for Regulation of Gut Immunity and Flora. Adv Sci (Weinh). 2021;8(18):e2101619.Https://doi.org/10.1002/advs.202101619
31. Azad AK, Al-Mahmood SMA, Chatterjee B, Wan Sulaiman WMA, Elsayed TM, Doolaanea AA. Encapsulation of Black Seed Oil in Alginate Beads as a pH-Sensitive Carrier for Intestine-Targeted Drug Delivery: In Vitro, In Vivo and Ex Vivo Study. Pharmaceutics. 2020;12(3).Https://doi.org/10.3390/pharmaceutics12030219
32. Niculescu AG, Grumezescu AM. Applications of Chitosan-Alginate-Based Nanoparticles-An Up-to-Date Review. Nanomaterials (Basel). 2022;12(2).Https://doi.org/10.3390/nano12020186
33. Volic M, Pajic-Lijakovic I, Djordjevic V, et al. Alginate/soy protein system for essential oil encapsulation with intestinal delivery. Carbohydr Polym. 2018;200:15-24.Https://doi.org/10.1016/j.carbpol.2018.07.033
34. Chu JN, Traverso G. Foundations of gastrointestinal-based drug delivery and future developments. Nat Rev Gastroenterol Hepatol. 2022;19(4):219-238.Https://doi.org/10.1038/s41575-021-00539-w
35. Zhang W, Liu C, Li J, et al. Tanshinone IIA: New Perspective on the Anti-Tumor Mechanism of A Traditional Natural Medicine. Am J Chin Med. 2022;50(1):209-239.Https://doi.org/10.1142/S0192415X22500070
36. Roach PJ. AMPK -> ULK1 -> autophagy. Mol Cell Biol. 2011;31(15):3082-3084.Https://doi.org/10.1128/MCB.05565-11
37. Hsu CC, Peng D, Cai Z, Lin HK. AMPK signaling and its targeting in cancer progression and treatment. Semin Cancer Biol. 2022;85:52-68.Https://doi.org/10.1016/j.semcancer.2021.04.006
38. Lee H, Zandkarimi F, Zhang Y, et al. Energy-stress-mediated AMPK activation inhibits ferroptosis. Nat Cell Biol. 2020;22(2):225-234.Https://doi.org/10.1038/s41556-020-0461-8

Figures

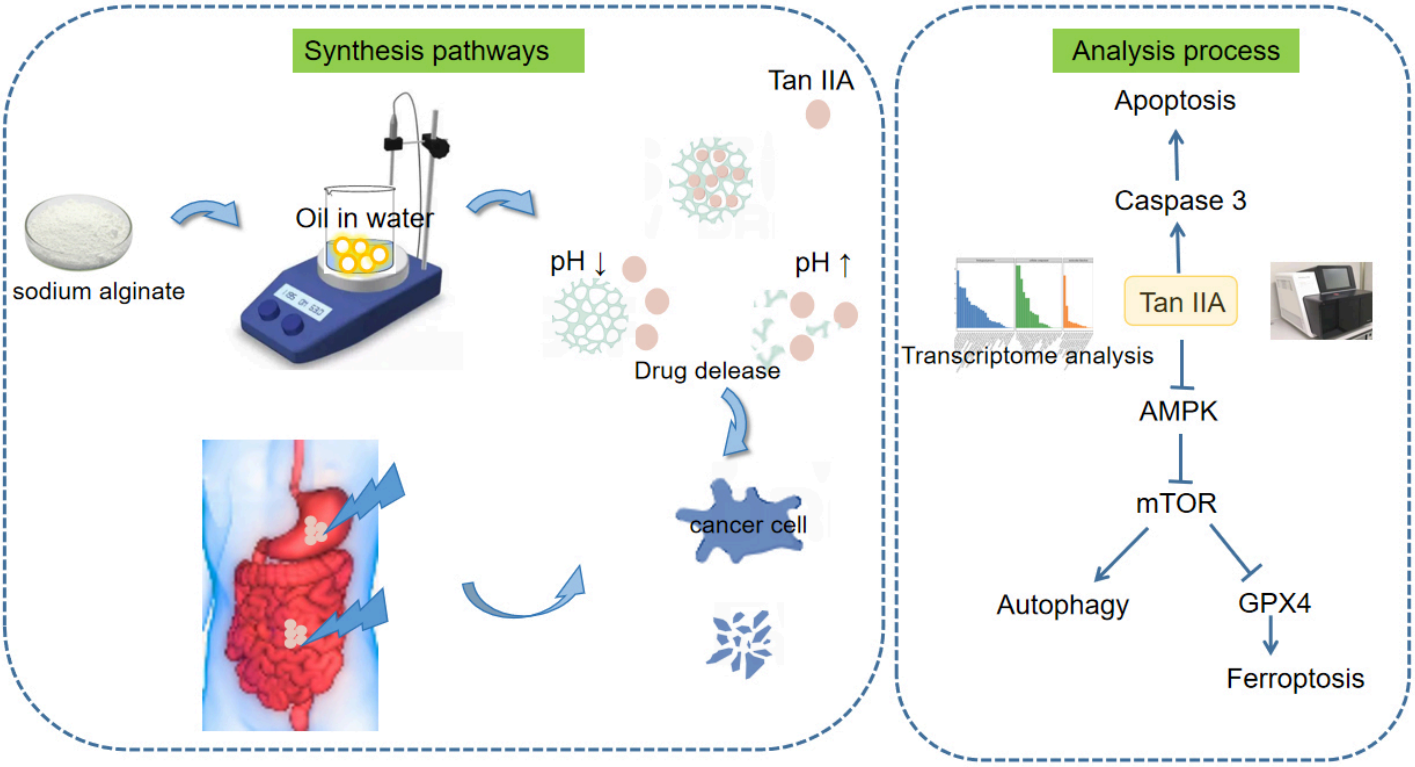


Figure 1

Schematic illustration depicting the fabrication process of Tan IIA/CA particles.

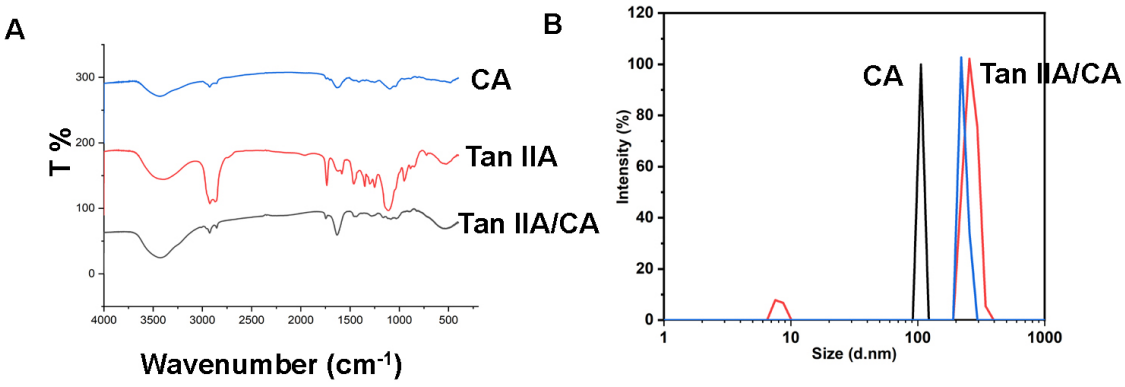


Figure 2

The characterization of particles, including the Fourier Transform Infrared (FTIR) spectra and their particle size (nm).

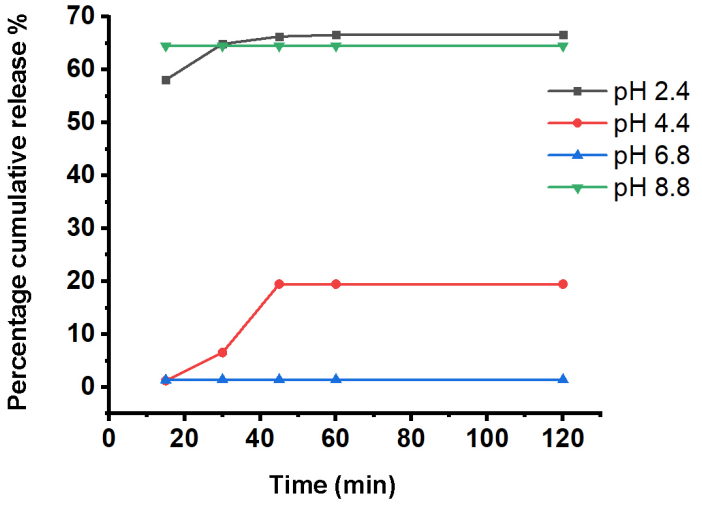


Figure 3

Release pattern of drug release in various pH solutions.

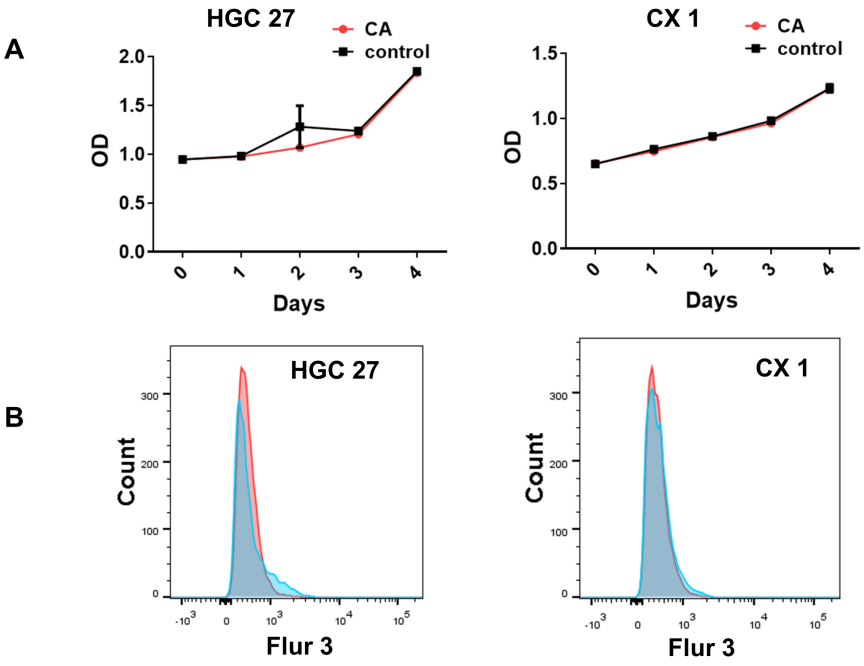


Figure 4

Non biological toxicity of CA particles were measured by CCK 8 assay and calcium concentration assay on cells. (A) CCK 8 assay of cells after being treated with CA particles for 4 days. (B) Flow cytometry assay of intracellular calcium ion (Ca^{2+}) concentration of cells after being treated with CA particles.

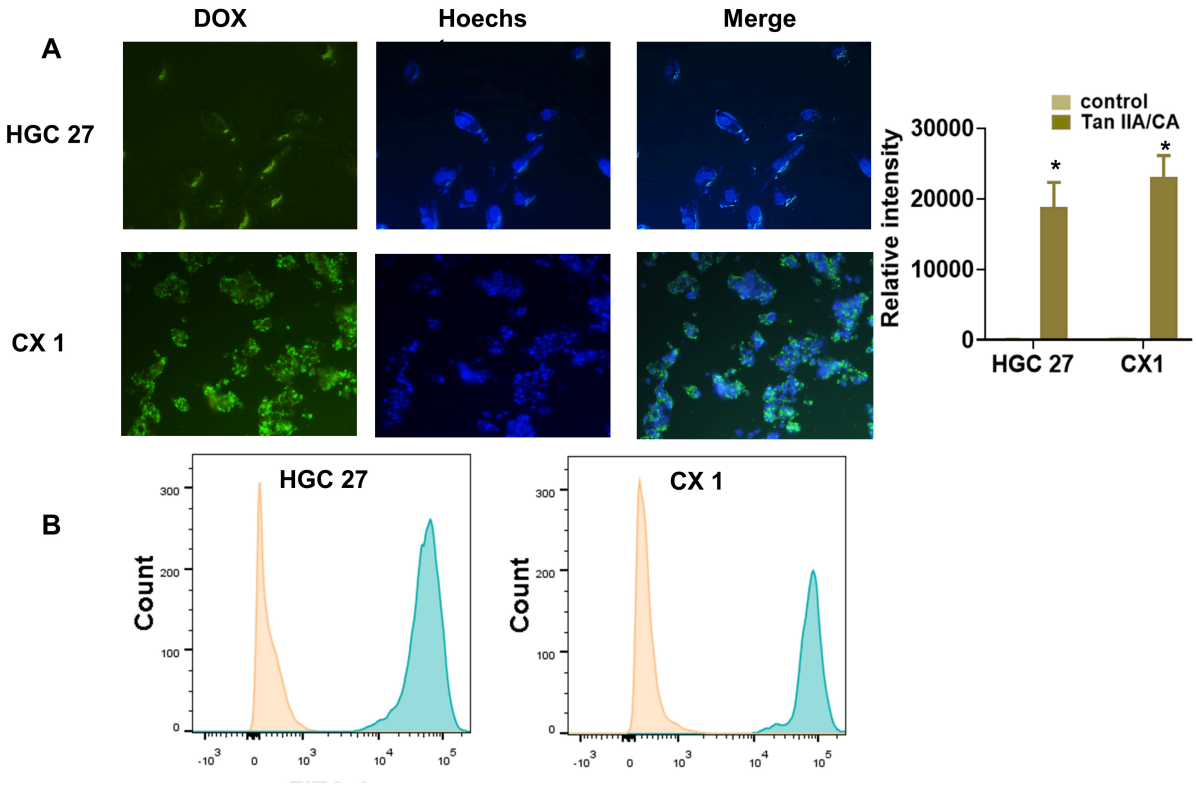


Figure 5

Cellular uptake were shown by confocal laser microscopy and flow cytotry in cells treated with Dox/CA particles. Quantification of fluorescent intensity were measured by Image J software. Data were shown as Mean ± SD. Experiments were performed in triplicate, *p<0.05, **p<0.01.

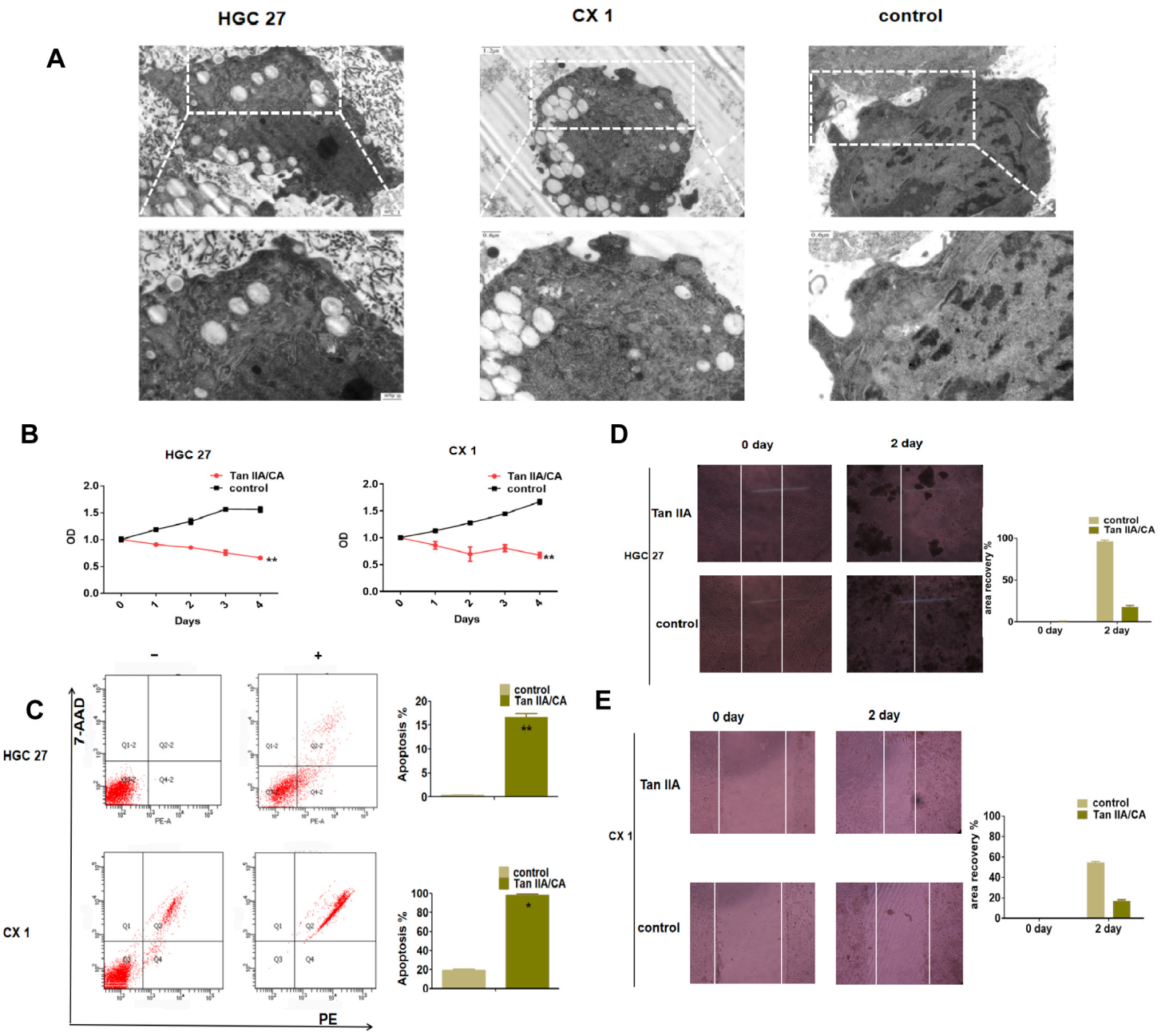


Figure 6

Comparisons of apoptosis levels in cells treated with Tan IIA/CA and control group. (A)The TEM images of particles size and distribution in cells (unit: nm). (B) Apoptosis was measured with CCK 8 kit. (C) Analysis of frequency of cell apoptosis using flow cytometry. Quantification of apoptosis percentage were shown as Mean ± SD. Experiments were performed in triplicate, *p<0.05, **p<0.01. (D) and (E) HGC 27 and CX 1 cells were treated with Tan IIA/CA particles and control and cell migration ability were assed with cell scratch assay. The image were taken at 0 day and 2 day after the gap were scratched. Quantification of relative recovery area is measured by Image J software. Data were shown as Mean ± SD. Experiments were performed in triplicate, *p<0.05, **p<0.01.

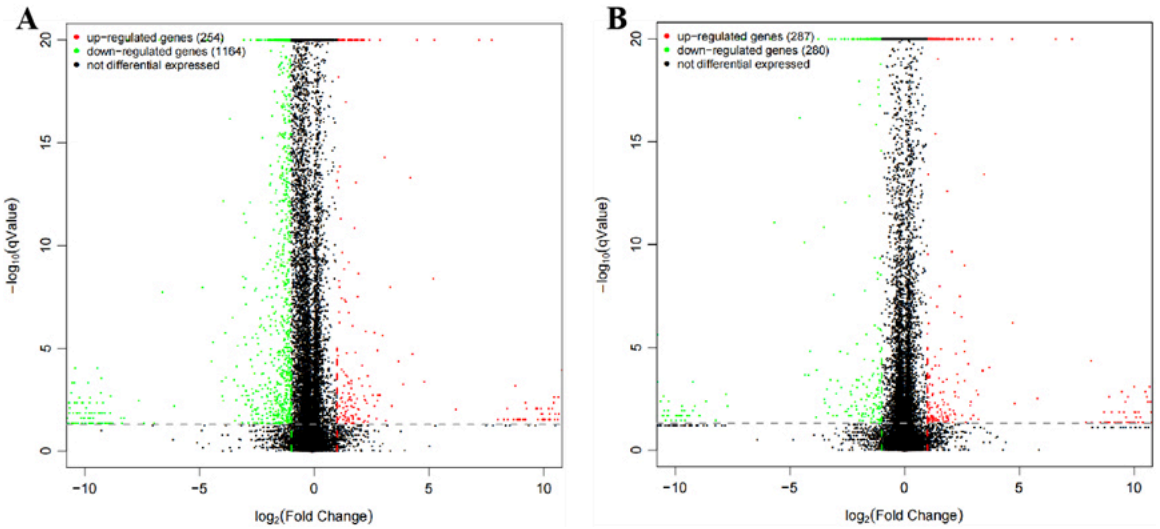


Figure 7

Volcano plot displaying the DEGs. (A) Volcano plot of DEGs in group HT vs H of HGC 27 cancer cells. (B)Volcano plot of DEGs in group CT vs C of CX 1 cancer cells. The X-axis indicates fold-change of gene expression (threshold, |log2 (Treat/Control) | > 1), while the Y-axis means the statistically significant level (threshold, p-value < 0.005). Red dots indicate groups of upregulated genes, green dots indicate groups of downregulated genes, and black dots indicate non-significantly differentially expressed genes (DEGs). Abbreviations: CT: CX 1 cells treated with Tan IIA/CA, HT: HGC 27 cells treated with Tan IIA/CA.

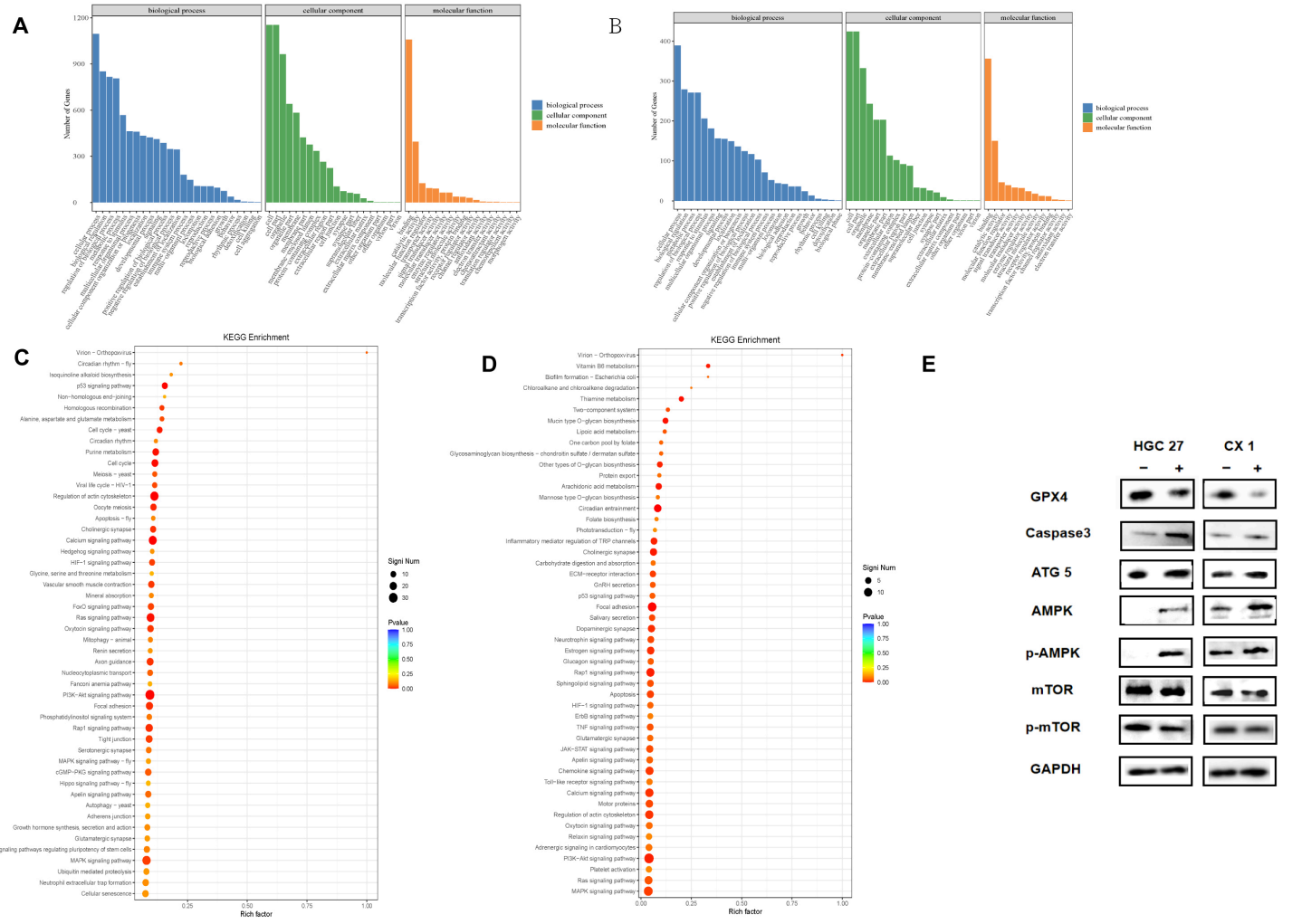


Figure 8

Functional enrichment analysis of DEGs. (A) The classification of Gene Ontology in group HT vs H of HGC 27 cancer cells. (B) The classification of Gene Ontology in group CT vs C of CX 1 cancer cells. (C) KEGG pathway enrichment in group HT vs H of HGC 27 cancer cells. (D) KEGG pathway enrichment in group CT vs C of CX1 cancer cells. Rich factor represents the ratio of the number of DEGs to the total number of annotated genes in this pathway. Abbreviations: CT: CX 1 cells treated with Tan IIA/CA, HT: HGC 27 cells treated with Tan IIA/CA. (E) Western blots were performed to evaluate the expression levels of ATG 5, GPX4, Caspase 3, AMPK, mTOR in HGC 27 and CX 1 cells following Tan II A/CA treatment, with GAPDH serving as the control. Experiments were performed in triplicate.Original blots/gels are presented in the supplementary document.